PHYSICAL REVIEW A **92**, 040303(R) (2015)

Universal control of an oscillator with dispersive coupling to a qubit

Stefan Krastanov,[1] Victor V. Albert,[1] Chao Shen,[1] Chang-Ling Zou,[1,2] Reinier W. Heeres,[1] Brian Vlastakis,[1] Robert J. Schoelkopf,[1] and Liang Jiang[1]

[1]*Departments of Applied Physics and Physics, Yale University, New Haven, Connecticut 06520, USA*

[2]*Key Lab of Quantum Information, University of Science and Technology of China, Hefei 230026, Anhui, China*

(Received 27 February 2015; published 21 October 2015)

We investigate quantum control of an oscillator mode off-resonantly coupled to an ancillary qubit. In the strong dispersive regime, we may drive the qubit conditioned on the number states of the oscillator, which, together with displacement operations, can achieve universal control of the oscillator. Based on our proof of universal control, we provide a straightforward recipe to perform arbitrary unitary operations on the oscillator. With the capability of universal control, we can significantly reduce the number of operations to prepare the number state $|n\rangle$ from $O(n)$ to $O(\sqrt{n})$. This universal control scheme of the oscillator enables us to efficiently manipulate the quantum information stored in the oscillator, which can be implemented using superconducting circuits.

DOI: 10.1103/PhysRevA.92.040303 PACS number(s): 03.67.−a, 03.65.Vf, 37.10.Jk, 42.50.Lc

As an important model for quantum information processing, the coupled qubit-oscillator system has been actively investigated in various platforms, including trapped ions [1], nanophotonics [2], cavity QED [3], and circuit QED [4]. Due to its convenient control, the physical qubit is usually the primary resource for quantum information processing. Meanwhile, the oscillator serves as an auxiliary system for quantum state transfer and detection [5]. In fact, the oscillator, associated with a phononic or photonic mode, may have long coherence times [1,6,7], and the large Hilbert space associated with the oscillator can be used for quantum encoding [8–10] and autonomous error correction with engineered dissipation [11]. These crucial features call for deeper investigations into quantum control theory of the oscillator.

The seminal work of Law and Eberly [12] has triggered many theoretical and experimental investigations to prepare the quantum states of the oscillator assisted by an ancillary qubit with Jaynes-Cummings (JC) coupling [1,13–15]. However, the more complex problem of implementing *arbitrary unitary operations* remains an outstanding challenge. Even with recent advances, protocols for universal control require either a large number of control operations [16], slow adiabatic transitions [17], or a more complicated model with an ancillary three-level system [18]. Meanwhile, the development of superconducting circuits acting in the strong dispersive regime opens new possibilities for universal control of the oscillator [19].

In this Rapid Communication, we provide a scheme for universal control of the oscillator assisted by an ancillary qubit. The scheme utilizes the dispersive Hamiltonian [19] along with two types of drives associated with the qubit and the oscillator, respectively. The key is the capability to drive the qubit [9,10,19–22] and impart arbitrary phases conditioned on the number state of the oscillator. An experimental implementation of the proposed scheme, confirming the feasibility of the protocol, is presented in Ref. [23].

The Hamiltonian of the qubit-oscillator system is

$$\hat{H} = \hat{H}_0 + \hat{H}_1 + \hat{H}_2, \tag{1}$$

with a dispersively coupled qubit and oscillator [19]

$$\hat{H}_0 = \omega_q |e\rangle\langle e| + \omega_c \hat{n} - \chi |e\rangle\langle e|\hat{n}, \tag{2}$$

time-dependent drive of the oscillator,

$$\hat{H}_1 = \epsilon(t) e^{i\omega_c t}\hat{a}^\dagger + \text{H.c.}, \tag{3}$$

and time-dependent drive of the qubit,

$$\hat{H}_2 = \Omega(t) e^{i\omega_q t}|e\rangle\langle g| + \text{H.c.} \tag{4}$$

Above, ω_q is the qubit transition frequency between $|g\rangle$ and $|e\rangle$, ω_c is the oscillator frequency, $\hat{a}^\dagger(\hat{a})$ are the raising (lowering) operators, $\hat{n} = \hat{a}^\dagger\hat{a}$ is the number operator of the oscillator, χ is the dispersive coupling, and $\Omega(t)$ and $\epsilon(t)$ are the time-dependent drives of the qubit and the oscillator, respectively. The eigenstates of $\hat{H}_0$ are $|g,n\rangle$ and $|e,n\rangle$ with an oscillator excitation number $n = 0,1,\ldots$, as illustrated in Fig. 1.

Our control scheme requires the following three constraints: (1) The oscillator and qubit are never driven simultaneously [i.e., $\epsilon(t)\Omega(t) = 0$ for all t]; (2) the qubit is in the ground state $|g\rangle$ whenever the oscillator drive is on [i.e., when $\epsilon(t) \neq 0$]; and (3) the qubit drive is weak compared with the dispersive coupling, i.e., $|\Omega(t)| \ll \chi$.

With the above constraints, we have two types of operations. Operations of type ① [based on Eq. (3) under constraint No. 2] are displacements,

$$\text{Type ①}: \hat{D}(\alpha) = \exp(\alpha\hat{a}^\dagger - \alpha^*\hat{a}), \tag{5}$$

with $\alpha = i\int \varepsilon(t)dt$, which can coherently pump or remove energy from the oscillator. Operations of type ② [based on Eq. (4) under constraint No. 3] are qubit rotations *conditional on the number states* [19–22,24], which can impart number-dependent Berry phases. As illustrated in Fig. 1, there is a series of transition frequencies of the qubit, $\{\omega_q - \chi n\}_{n=0}^{\infty}$, depending on the excitation number of the oscillator. We can achieve unitary rotations between the selected levels $\{|g,n\rangle,|e,n\rangle\}$ with a negligible effect on the rest of the system, if we drive the qubit with $\Omega(t) = \Omega_n(t)e^{-in\chi t}$ and $|\Omega_n| \ll \chi$ [19–22]. Hence, we can impart a Berry phase to a selected number state: $|g,n\rangle \to e^{i\theta_n}|g,n\rangle$, with θ_n proportional to the solid angle subtended by the path in the Bloch sphere associated with $\{|g,n\rangle,|e,n\rangle\}$ (as illustrated in Fig. 1). Since

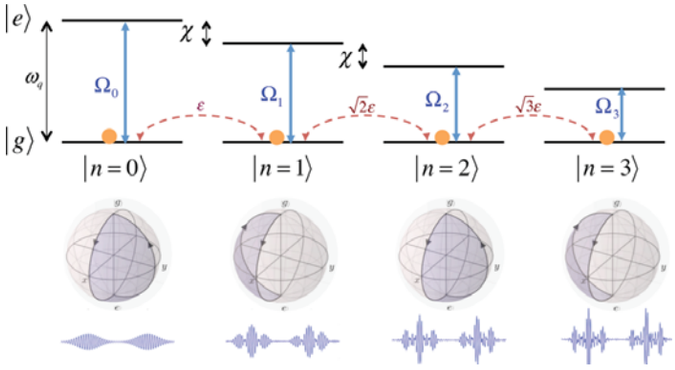

FIG. 1. (Color online) Energy-level diagram of the qubit-oscillator system. In the rotating frame of the oscillator, the states $\{|g,n\rangle\}_n$ have the same energy. After each operation, the population (orange circles) remains in the subspace associated with $|g\rangle$. A weak displacement operation (red dashed arrows) couples the states $|g,n-1\rangle$ and $|g,n\rangle$ with strength $\sqrt{n}\varepsilon$ for all n. The SNAP gate (blue solid arrows) can simultaneously accumulate different Berry phases $\{\theta_n\}$ to states $\{|g,n\rangle\}$. The Berry phase θ_n is proportional to the enclosed shaded area in the corresponding Bloch sphere, achieved by resonant microwave pulses with frequency $\omega_q - n\chi$ (blue oscillatory fields).

the qubit remains in $|g\rangle$ after the operation, we can effectively obtain a *selective number-dependent arbitrary phase* (SNAP) operation

$$\hat{S}_n(\theta_n) = e^{i\theta_n|n\rangle\langle n|}, \tag{6}$$

which imparts phase θ_n to the number state $|n\rangle$. Since the excitation number is preserved during the SNAP operation (due to constraint No. 1), we may drive the qubit with multiple frequency components, $\Omega(t) = \sum_n \Omega_n(t)e^{i(\omega_q - \chi n)t}$. These will simultaneously accumulate different phases θ_n for different number states and implement the general SNAP gate,

$$\text{Type ②}: \ \hat{S}(\vec{\theta}) = \prod_{n=0}^{\infty} \hat{S}_n(\theta_n) = \sum_{n=0}^{\infty} e^{i\theta_n}|n\rangle\langle n|, \tag{7}$$

where $\vec{\theta} = \{\theta_n\}_{n=0}^{\infty}$ is the list of phases. Since θ_n can be an arbitrary function of n, the SNAP gate can simulate arbitrary nonlinear effects that conserve the excitation number. For example, if we choose $\theta_n \propto n^2$, the SNAP gate effectively induces a Kerr nonlinearity of the oscillator. With SNAP gates, we just need to consider real displacement, because any complex displacement $\alpha = re^{i\phi}$ can be decomposed as a real displacement conjugated by a SNAP gate, $\hat{D}(\alpha) = \hat{S}(\vec{\theta})\hat{D}(r)\hat{S}(-\vec{\theta})$ with $\theta_n = n\phi (\text{mod } 2\pi)$.

Proof of universality. To show that the operations $\hat{D}(\alpha)$ and $\hat{S}(\vec{\theta})$ are sufficient for universal control of the oscillator, we first identify $\hat{p} = -i(\hat{a}^\dagger - \hat{a})$ as a generator of $\hat{D}(\alpha)$ for real α, and $\{\hat{Q}_n = \sum_{n'=0}^{n}|n'\rangle\langle n'|\}_n$ as generators of $\hat{S}(\vec{\theta})$. Their commutator is

$$\hat{J}_n = i[\hat{p},\hat{Q}_n] = \sqrt{n+1}(|n\rangle\langle n+1| + |n+1\rangle\langle n|),$$

which can selectively couple n and $n-1$. This gives the group commutator

$$\hat{D}(\epsilon)\hat{R}_n(\epsilon)\hat{D}(-\epsilon)\hat{R}_n(-\epsilon) = \exp[iJ_n\epsilon^2 + O(\epsilon^3)], \tag{8}$$

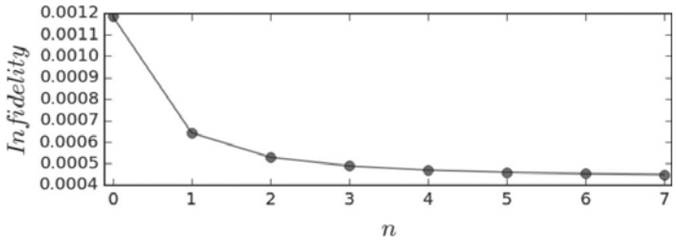

FIG. 2. Plot of infidelity of the unitary $\hat{V}_n$ [Eq. (10)] constructed by our protocol with respect to the desired target unitary $\hat{V}_{n,\text{target}}$ [Eq. (9)] vs n. The target unitaries are $\frac{\pi}{2}$ rotations on the $\{|n\rangle,|n+1\rangle\}$ subspace. In the limit of $|\Omega_n|/\chi \to 0$, the simple implementation of Eq. (10) can already achieve fidelities $F = \frac{1}{2}|\text{Tr}(\hat{V}_n^\dagger \hat{V}_{n,\text{target}})|$ of better than 0.998. In the calculation of the fidelity we use the 2×2 submatrices of interest (acting on the $\{|n\rangle,|n+1\rangle\}$ subspace).

for small real ϵ and for the SNAP gate,

$$\hat{R}_n(\epsilon) = e^{i\hat{Q}_n\epsilon} = \hat{S}(\{\epsilon,\ldots\epsilon,0,\ldots\}) = \sum_{n'=0}^{n} e^{i\epsilon}|n'\rangle\langle n'| + \sum_{n'=n+1}^{\infty}|n'\rangle\langle n'|.$$

For any integer $N > 0$, $\{\hat{J}_n\}_{n=0}^{N-1}$ and $\{\hat{Q}_n\}_{n=0}^{N-1}$ are sufficient to generate the Lie algebra $\mathfrak{u}(N)$ over the truncated number space spanned by $\{|n\rangle|n < N\}$, which implies universal control of the oscillator [25–27].

Explicit construction of target unitary. Let us first consider the elementary target unitary operation

$$\hat{V}_{n,\text{target}} = \cos\theta(|n\rangle\langle n| + |n+1\rangle\langle n+1|) + \sin\theta(|n\rangle\langle n+1| - |n+1\rangle\langle n|) \tag{9}$$

that performs a rotation of angle θ in the $\{|n\rangle,|n+1\rangle\}$ subspace, with an efficient approximate implementation

$$\hat{V}_n = \hat{D}\left(\alpha_1^{(n)}\right)\hat{R}_n(\pi)\hat{D}\left(\alpha_2^{(n)}\right)\hat{R}_n(\pi)\hat{D}\left(\alpha_3^{(n)}\right), \tag{10}$$

where $\hat{R}_n(\pi) = -\sum_{n'=0}^{n}|n'\rangle\langle n'| + \sum_{n'=n+1}^{\infty}|n'\rangle\langle n'|$ is a SNAP gate with a π phase shift for number states with no more than n excitations. It is important to impose the constraint $\alpha_1 + \alpha_2 + \alpha_3 = 0$ to minimize the undesired effects to the subspace associated with $|n'\rangle \neq |n\rangle$ or $|n+1\rangle$. Numerically, we optimize the fidelity, $F = \frac{1}{N_c}|\text{Tr}(\hat{V}_n^\dagger \hat{V}_{n,\text{target}})|$, where N_c is the cutoff dimension (i.e., the size of the matrices used to represent the operators) [28,29]. The numerical optimum is attained with $(\alpha_1,\alpha_2,\alpha_3) = (\alpha,-2\alpha,\alpha)$ (naturally, the value of α will depend on n and the angle of rotation). Figure 2 shows the infidelities we obtain using this protocol for the implementation of a $\frac{\pi}{2}$ rotation on $\{|n\rangle,|n+1\rangle\}$.

To construct an arbitrary target unitary $\hat{U}_{\text{target}}$ in the $\{|0\rangle,\ldots,|n-1\rangle\}$ subspace, we start by taking its inverse,

$$\hat{U}_{\text{target}}^{-1} = \left(\begin{array}{c|c} \hat{W}_n & 0 \\ \hline 0 & \hat{I}_{N_c-n} \end{array}\right),$$

where $\hat{W}_n$ is the nontrivial block and $\hat{I}_{n'}$ is the $n'\times n'$ identity matrix. We first apply a SNAP gate such that the last column of the $\hat{W}_n$ block now contains only non-negative coefficients. We then apply $n-1$ consecutive SO(2) rotations eliminating the off-diagonal elements in the last column of $\hat{W}_n$, such that

the column becomes $(0,\ldots,0,1)_n^{\mathsf{T}}$. Since all rows of a unitary matrix are orthonormal, the last row of the $\hat{W}_n$ block must be transformed to $(0,\ldots,0,1)_n$. Hence, the result is

$$\hat{V}_{n-1}^{(n)}\hat{V}_{n-2}^{(n)}\cdots\hat{V}_0^{(n)}\hat{S}^{(n)}\hat{U}_{\text{target}}^{-1}=\left(\begin{array}{c|c|c}\hat{W}_{n-1} & 0 & 0\\ \hline 0 & 1 & 0\\ \hline 0 & 0 & I_{N_c-n}\end{array}\right),$$

where $\hat{S}^{(n)}$ is a SNAP gate necessary for any complex phases unobtainable with the SO(2) operations. The $n-1$SO(2) rotations,

$$\hat{V}_k^{(n)}=\hat{D}\big(\alpha_k^{(n)}\big)\hat{R}_k(\pi)\hat{D}\big(-2\alpha_k^{(n)}\big)\hat{R}_k(\pi)\hat{D}\big(\alpha_k^{(n)}\big),$$

can be individually optimized, before being chained together for a second round of optimization over $n-1$ displacement parameters $\{\alpha_k^{(n)}\}_{k=0}^{n-1}$. The cost function to be minimized for the second round of optimization is the sum of absolute values of off-diagonal terms (excluding the $\hat{W}_{n-1}$ block). We iterate the procedure until we obtain

$$\hat{U}_{\text{construct}}\hat{U}_{\text{target}}^{-1}\approx\hat{I}, \tag{11}$$

with $\hat{U}_{\text{construct}}=\prod_{n'=1}^{n}(\hat{V}_{n'-1}^{(n')}\hat{V}_{n'-2}^{(n')}\cdots\hat{V}_0^{(n')}\hat{S}^{(n')})$, as illustrated in Figs. 3(a) and 3(b) for a specific U_{target} [30].

Using the above decomposition, we need $n(n-1)/2$ SO(2) rotations (each containing three displacements and two SNAP gates). We can combine consecutive displacements, lowering the number of displacements to two per SO(2) rotation. We also need one SNAP gate at each iteration of the $\hat{W}_n\rightarrow\hat{W}_{n-1}$ step, with a total of n additional SNAP gates. For various $\hat{U}_{\text{target}}$, as illustrated in Figs. 3(c) and 3(d), we find that the stepwise optimization procedure can yield a good final fidelity $F=\frac{1}{N_c}|\text{Tr}(\hat{U}_{\text{construct}}^{\dagger}\hat{U}_{\text{target}})|>0.99$, which can be further improved to $F>0.999$ with a third round of simultaneous optimizations over all $n(n-1)/2$ displacement parameters $\{\alpha_k^{(n')}\}_{k<n'\leqslant n}$.

Our scheme can be applied to the general Hamiltonian with dispersive coupling, $-\sum_n\chi_n|e,n\rangle\langle e,n|$, as long as the number-dependent qubit frequency shift can be resolved [$|\chi_n-\chi_{n'\neq n}|\gg|\Omega(t)|,\gamma,\kappa$, for all relevant n and n', where γ and κ are the qubit and cavity decoherence rates, respectively]. Furthermore, we can also extend the arbitrary unitary control to the subspaces spanned by $\{|g,n'\rangle,|e,n'\rangle\}_{n'=0}^{n-1}$, so that we can control the entire $2n$-dimensional quantum system [31].

Sublinear scheme to prepare the number state. The preparation of an arbitrary target state starting from the vacuum is a special case of the above protocol where we constrain only the first column of the target matrix. To prepare a state in the $\{|0\rangle,\ldots|n\rangle\}$ subspace, such an operation will require only $O(n)$ operations instead of the $O(n^2)$ operations discussed above. However, certain states with a narrow distribution of photon numbers can be prepared even more efficiently by taking advantage of the fast, experimentally available displacement operations. For example, the preparation of the number state $|n\rangle$ requires $O(n)$ sequential SO(2) rotations from $|0\rangle$ using the generic scheme. In contrast, if we start from the coherent state $\hat{D}(\alpha)|0\rangle=|\alpha\rangle$ with $\alpha=\sqrt{n}$, whose population distribution is centered around $|n\rangle$ with a spread of $O(\sqrt{n})$, we need only $O(\sqrt{n})$ rounds of SO(2) rotations to "fold" the coherent state $|\alpha\rangle$ to the number state $|n\rangle$. Figure 4 compares the number of SNAP gates needed between the generic linear scheme [with $O(n)$ operations] and the specialized sublinear schemes [with $O(\sqrt{n})$ operations] designed for the preparation of $|n\rangle$ from $|0\rangle$, with various target fidelities. For $n\gtrsim 8$, it becomes advantageous to use the specialized sublinear scheme instead of the generic scheme.

Imperfections. In the limiting case of $|\Omega_n/\chi|\rightarrow 0$, the SNAP gate can achieve the ideal unitary evolution as shown Eq. (7). In practice, however, $|\Omega_n/\chi|$ is finite and introduces deviations from the SNAP gate (e.g., undesired ac Stark shift).

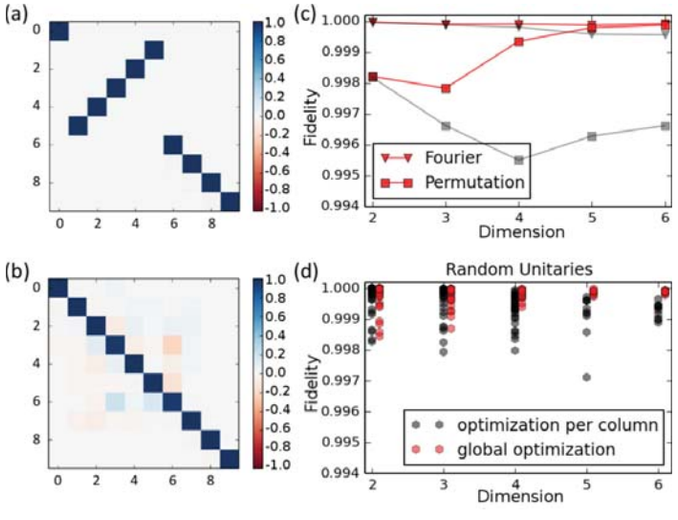

FIG. 3. (Color online) (a) An example target unitary operation, U_{target} (a permutation). (b) The product is close to identity, $\hat{U}_{\text{construct}}\hat{U}_{\text{target}}^{-1}\approx\hat{I}$, with small nonzero off-diagonal elements. (c), (d) Comparison of fidelities $F=\frac{1}{N_c}|\text{Tr}(\hat{U}_{\text{construct}}^{\dagger}\hat{U}_{\text{target}})|$ after column-nwise optimization (black) and fidelities with additional optimization over all displacement parameters (red) for (c) Fourier (triangles) and permutation (squares) operations and (d) randomly generated target unitary operations (hexagons).

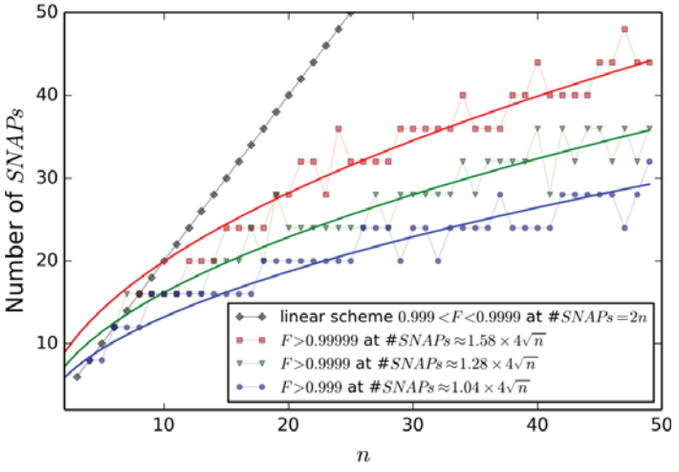

FIG. 4. (Color online) The number of SNAP gates for the preparation of $|n\rangle$ from $|0\rangle$ (with a fixed lower bound of fidelity) for a generic linear scheme (black diamond line) and specialized sublinear schemes with different target fidelities (colored lines). The specialized schemes operate on $\hat{D}(\sqrt{n})|0\rangle$ by folding all population from the subspace $\{|n-\Delta n\rangle,\ldots,|n+\Delta n\rangle\}$ to the number state $|n\rangle$.

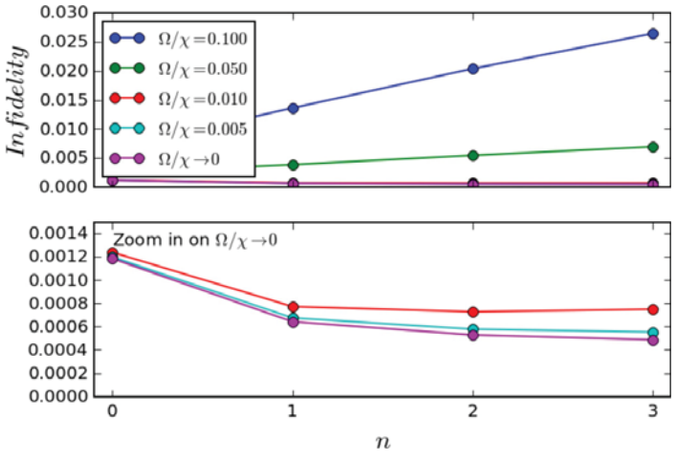

FIG. 5. (Color online) Reprise of Fig. 2 with finite values for Ω (represented in units of χ). The lower panel zooms in on smaller values for Ω. It is possible to achieve fidelities better than 0.99 for practical values of $\Omega = 0.05\chi$.

To calibrate such deviations, we simulate the full evolution of the gate from Eq. (10) based on a numerical integration of the original time-dependent Hamiltonian [Eq. (1)], and calculate the infidelity with respect to the target unitary [32], as illustrated in Fig. 5. We use realistic parameters from the experiment that implements the SNAP gate [23] ($\chi = 8.3$ MHz, $\omega_q = 7.6$ GHz, $\omega_c = 8.2$ GHz). We find that the SNAP gate is robust against such small imperfections, which scale as $O(|\Omega_n/\chi|^2)$ for square pulses. In principle, the unitary deviation due to finite $|\Omega_n/\chi|$ can be compensated using shaped or composite pulses [33]. In practice, with numerical optimization, it is possible to compensate both ac Stark shift and all higher-order corrections, which enables even faster operation with $\Omega(t) \sim \chi$ [21,22,34].

Discussions. We now compare our SNAP-gate-based quantum control scheme with previous protocols. The scheme proposed by Law and Eberly [12] is based on the JC model, $H_{\rm JC} \propto \hat{a}|e\rangle\langle g| + \text{H.c.}$, which enables preparation of arbitrary superpositions of number states. The scheme by Mischuck and Molmer [16] further extended the JC model from state preparation to arbitrary unitary operation, but it is rather complicated because any JC control pulse necessarily couples the states $|g,n\rangle$ and $|e,n-1\rangle$ (for all n) simultaneously and with varying strength $g\sqrt{n}$. In contrast, our scheme is based on the dispersive qubit-oscillator coupling, $H_{\rm dispersive} = -\chi|e\rangle\langle e|\hat{n}$, which preserves the oscillator number states, enables the SNAP gate to directly access the two selected sublevels $|g,n\rangle$ and $|e,n\rangle$ with negligible effects on the rest of the levels, and ultimately leads to efficient universal control of the oscillator. Another protocol for the JC Hamiltonian is presented by Strauch in Ref. [17], however, it requires a slow adiabatic transition between coupled and uncoupled cavity states. The proposal by Santos [18] introduces a different model with a three-level Λ-type ancillary system to achieve universal control, but it is experimentally more challenging than the simple two-level ancilla considered in our scheme.

With dispersive qubit-oscillator coupling, there are other control protocols available. For example, in the presence of the oscillator drive ϵ, we may "block" the processes $|n' \pm 1\rangle \to |n'\rangle$ by driving the qubit resonantly to the transition $|g,n'\rangle \leftrightarrow |e,n'\rangle$, with $\Omega_{n'} \gg \epsilon\sqrt{n'}$ [35]. Similarly, by resonantly driving transitions $|g,n'\rangle \leftrightarrow |e,n'\rangle$ for $n' < n$ and $n' > n+1$, we block all number changing transitions, except for the transition between $\{|n\rangle, |n+1\rangle\}$ that can be used for SO(2) unitary rotations. This blockade scheme is relatively slow and each elementary operation takes time $\tau \sim (\epsilon\sqrt{n})^{-1} \gg \Omega^{-1} \gg \chi^{-1}$ due to the blockade requirements, while the SNAP-gate-based scheme can be much faster with $\tau \sim \chi^{-1}$.

In conclusion, the SNAP-gate-based scheme provides universal control of the oscillator mode with strong dispersive coupling to a qubit. Based on the proof of universal control, we show explicit constructions for arbitrary state preparation and arbitrary unitary operation of the oscillator. We also present an efficient procedure to prepare the number state $|n\rangle$ using only $O(\sqrt{n})$ operations. We note that deterministic SNAP-gate-based preparation of the $|n = 1\rangle$ photon number state has been demonstrated using superconducting circuits [23]. The techniques introduced here are not restricted to oscillator modes such as mechanical motions [1] and optical or microwave cavities [2–4] and can be extended to multilevel systems such as Rydberg atoms with large angular momentum [35], as long as the dispersive coupling between the qubit and oscillator or multilevel system is strong.

We thank Michel H. Devoret, Luigi Frunzio, Steven M. Girvin, Zaki Leghtas, Mazyar Mirrahimi, Andrei Petrenko, and Matthew Reagor for helpful discussions. The work was supported by ARO, AFOSR MURI, DARPA Quiness program, NBRPC 973 program, the Alfred P. Sloan Foundation, and the Packard Foundation. V.V.A. acknowledges support from NSF GRFP (DGE-1122492). We thank the Yale High Performance Computing Center for use of their resources.

[1] D. Leibfried, R. Blatt, C. Monroe, and D. Wineland, Rev. Mod. Phys. **75**, 281 (2003).

[2] T. G. Tiecke, J. D. Thompson, N. P. de Leon, L. R. Liu, V. Vuletic, and M. D. Lukin, Nature (London) **508**, 241 (2014).

[3] A. Reiserer, N. Kalb, G. Rempe, and S. Ritter, Nature (London) **508**, 237 (2014).

[4] M. H. Devoret and R. J. Schoelkopf, Science **339**, 1169 (2013).

[5] R. J. Schoelkopf and S. M. Girvin, Nature (London) **451**, 664 (2008).

[6] T. A. Palomaki, J. W. Harlow, J. D. Teufel, R. W. Simmonds, and K. W. Lehnert, Nature (London) **495**, 210 (2013).

[7] M. Reagor, H. Paik, G. Catelani, L. Y. Sun, C. Axline, E. Holland, I. M. Pop, N. A. Masluk, T. Brecht, L. Frunzio, M. H. Devoret, L. Glazman, and R. J. Schoelkopf, Appl. Phys. Lett. **102**, 192604 (2013).

[8] D. Gottesman, A. Kitaev, and J. Preskill, Phys. Rev. A **64**, 012310 (2001).

[9] Z. Leghtas, G. Kirchmair, B. Vlastakis, M. H. Devoret, R. J. Schoelkopf, and M. Mirrahimi, Phys. Rev. A **87**, 042315 (2013).
[10] Z. Leghtas, G. Kirchmair, B. Vlastakis, R. J. Schoelkopf, M. J. Devoret, and M. Mirrahimi, Phys. Rev. Lett. **111**, 120501 (2013).
[11] M. Mirrahimi, Z. Leghtas, V. V. Albert, S. Touzard, R. Schoelkopf, L. Jiang, and M. Devoret, New J. Phys. **16**, 045014 (2014).
[12] C. K. Law and J. H. Eberly, Phys. Rev. Lett. **76**, 1055 (1996).
[13] S. Brattke, B. T. H. Varcoe, and H. Walther, Phys. Rev. Lett. **86**, 3534 (2001).
[14] A. A. Houck, D. I. Schuster, J. M. Gambetta, J. A. Schreier, B. R. Johnson, J. M. Chow, L. Frunzio, J. Majer, M. H. Devoret, S. M. Girvin, and R. J. Schoelkopf, Nature (London) **449**, 328 (2007).
[15] M. Hofheinz, H. Wang, M. Ansmann, R. C. Bialczak, E. Lucero, M. Neeley, A. D. O'Connell, D. Sank, J. Wenner, J. M. Martinis, and A. N. Cleland, Nature (London) **459**, 546 (2009).
[16] B. Mischuck and K. Molmer, Phys. Rev. A **87**, 022341 (2013).
[17] F. W. Strauch, Phys. Rev. Lett. **109**, 210501 (2012).
[18] M. F. Santos, Phys. Rev. Lett. **95**, 010504 (2005).
[19] D. I. Schuster, A. A. Houck, J. A. Schreier, A. Wallraff, J. M. Gambetta, A. Blais, L. Frunzio, J. Majer, B. Johnson, M. H. Devoret, S. M. Girvin, and R. J. Schoelkopf, Nature (London) **445**, 515 (2007).
[20] B. R. Johnson, M. D. Reed, A. A. Houck, D. I. Schuster, L. S. Bishop, E. Ginossar, J. M. Gambetta, L. DiCarlo, L. Frunzio, S. M. Girvin, and R. J. Schoelkopf, Nat. Phys. **6**, 663 (2010).
[21] B. Vlastakis, G. Kirchmair, Z. Leghtas, S. E. Nigg, L. Frunzio, S. M. Girvin, M. Mirrahimi, M. H. Devoret, and R. J. Schoelkopf, Science **342**, 607 (2013).
[22] S. E. Nigg, Phys. Rev. A **89**, 022340 (2014).
[23] R. W. Heeres, B. Vlastakis, E. Holland, S. Krastanov, V. V. Albert, L. Frunzio, L. Jiang, and R. J. Schoelkopf, Phys. Rev. Lett. **115**, 137002 (2015).
[24] S. E. Nigg and S. M. Girvin, Phys. Rev. Lett. **110**, 243604 (2013).
[25] S. Lloyd and S. L. Braunstein, Phys. Rev. Lett. **82**, 1784 (1999).
[26] S. L. Braunstein and P. van Loock, Rev. Mod. Phys. **77**, 513 (2005).
[27] K. Jacobs, Phys. Rev. Lett. **99**, 117203 (2007).
[28] N. Khaneja, T. Reiss, C. Kehlet, T. Schulte-Herbruggen, and S. J. Glaser, J. Magn. Reson. **172**, 296 (2005).
[29] This definition of fidelity is slightly faster to calculate than the definition with uniform norm, but, more importantly, it permits analytic expressions for the gradient of the cost function, greatly speeding up the optimization algorithm.
[30] The SCIPY routines were used for numerical optimizations.
[31] S. Krastanov (unpublished).
[32] See Supplemental Material at http://link.aps.org/supplemental/10.1103/PhysRevA.92.040303 for details on the numerical approach used for verification.
[33] L. M. K. Vandersypen and I. L. Chuang, Rev. Mod. Phys. **76**, 1037 (2005).
[34] R. W. Heeres (unpublished).
[35] A. Signoles, A. Facon, D. Grosso, I. Dotsenko, S. Haroche, J.-M. Raimond, M. Brune, and S. Gleyzes, Nat. Phys. **10**, 715 (2014).